Received: 4 September 2024 | Revised: 22 November 2024 | Accepted: 12 December 2024

IET Microwaves, Antennas & Propagation

DOI: 10.1049/mia2.12543

ORIGINAL RESEARCH

A miniaturised frequency selective rasorber with wide transmission band

Ruofeng Xu[1] | Jing Wang[1] | Xianglin Kong[1] | Bingmei Zhang[1] | Jun Wang[1] | Shengjun Zhang[2] | Xiaochun Liu[3] | Lei Zhao[1]

[1]School of Information and Control Engineering, China University of Mining and Technology, Xuzhou, China

[2]Test Physics & Numerical Mathematical, National Key Laboratory of Science and Technology, Beijing, China

[3]Key Laboratory of Aeronautical Science and Technology, Jinan, China

Correspondence

Lei Zhao.
Email: leizhao@cumt.edu.cn

Funding information

National Natural Science Foundation of China, Grant/Award Numbers: 51507176, 61771226, 62201575

Abstract

This paper demonstrates a miniaturised frequency selective rasorber (FSR) that incorporates meander cross-rings to realise a wide transmission band. The FSR comprises a resistive layer and a bandpass frequency selective surface (FSS), which are separated by an air layer. The resistive layer is constructed by employing meander cross-rings equipped with lumped resistances, where the inner arms of cross-rings are bent to obtain a parallel resonant circuit with large inductances and small capacitances to achieve broadband transmission at high frequencies. The bandpass FSS is implemented using a triple-layer metallic structure, where two identical square ring layers are coupled through a central metal grid layer to form the transmission band. The measured results indicate that the absorption band with absorptance exceeding 90% is from 3.5 to 9.4 GHz, and the passband exhibiting insertion loss of less than 1 dB spans from 11.92 to 17.98 GHz with a 40.5% relative bandwidth, which matches well with simulated ones. This FSR has the characteristics of simple structure and high performance, which provides a novel concept of stealth applications.

KEYWORDS

frequency selective surfaces, radar absorbing materials

1 | INTRODUCTION

The progressive development of stealth technology has generated heightened attention towards frequency selective rasorber (FSR). The FSR can transmit electromagnetic waves (EMs) in the band and absorb EMs outside the band to reduce all-around electromagnetic scattering. In recent decades, a host of new FSR structures has been proposed. The classification of FSRs into three categories is determined by the spatial relationship between absorption and transmission bands. These categories are as follows: FSRs characterised by a transmission band located below the absorption band [1–4], FSRs characterised by a transmission band located above the absorption band [5, 6], and FSRs characterised by a transmission band situated within the midst of the absorption bands [7–12].

Despite the excellent absorption performance of the mentioned FSRs, their transmission capabilities suffer from limited bandwidth. Given the utilisation of array systems [13–15] in modern radar antennas, which exhibit exceptional performance in broadband, the antennas are specifically designed to operate effectively across a broad spectrum of frequencies. In order to receive or transmit signals in the operating frequency band, the FSR as a radar radome needs to have the characteristics of broadband transmission. In the FSR, comprising a top resistive layer and a bottom bandpass frequency selective surface (FSS) layer, it is essential for both layers to possess a wide transmission window to realise broadband transmission. The research on broadband FSSs has been relatively mature. For the resonant FSS structure, the multilayer cascaded structure can be used to expand the bandwidth [16]; for the non-resonant structure, the complementary characteristics of the structure and related parameters were used to expand the bandwidth [17]. But few studies focus on how to make the resistive layer obtain a wide transmission

window. In ref. [18], it was proposed to insert a circular spiral resonator into the central position of a hexagonal metal loop with a lumped resistance to generate a wide transmission window. In ref. [19], it was proposed to insert a convoluted resonator in the central position of the metal dipole with lumped resistance to get broadband transmission characteristics. However, the designs and manufactures of resonators in refs. [18, 19] were complicated.

This paper presents the design process of FSR, which has the broadband characteristics of transmissions at higher-frequency band and absorptions at lower-frequency band. The FSR achieves a transmission band in where the insertion loss (IL) is less than 1 dB, spanning from 12.22 to 17.93 GHz, and an absorption band with absorptance exceeding 90% in the region of 3.66–9.8 GHz. The transmission and absorption performance of FSR indicates excellent stability within a 30° incident angle. Moreover, the prototype was fabricated and tested, confirming the consistency between the simulated and measured results.

2 | DESIGN AND ANALYSIS

This section details the design process of the absorber in a comprehensive manner. The equivalent circuit model (ECM) in Section 2.1 is used to represent the transmission bands, where impedance values are manipulated to achieve optimal transmission characteristics. Section 2.2 demonstrates the resistive layer design, which causes the miniaturisation of the structure and enhances the bandwidth. Section 2.3 introduces a triple-layer FSS, which is designed to match the resistive layer's transmission characteristics.

2.1 | The achievement of wide transmission band

Figure 1 illustrates the representation of the ECM pertaining to the multilayer FSR. Z_0 represents the characteristic impedance of free space, while Z_R and Z_F represent the equivalent impedance of the resistive layer and bandpass FSS correspondingly. Regarding the bandpass FSS, the value of Z_F can be considered infinite within the passband. Therefore, the transmission coefficient between the two ports can be formulated as follows:

$$|S_{21}| \xrightarrow{Z_F \to \infty} \frac{2}{|2 + Z_0/Z_R|} \tag{1}$$

Ideally, the transmission coefficient is equal to 1 when the value of Z_R approaches infinity. However, this situation is only feasible at a specific frequency point in parallel resonance and not attainable across a wide range of frequencies. Fortunately, broadband transmission can be realised under certain standards, such as $|S_{21}| > -0.5$ dB (≈ 0.9). When the real part R of

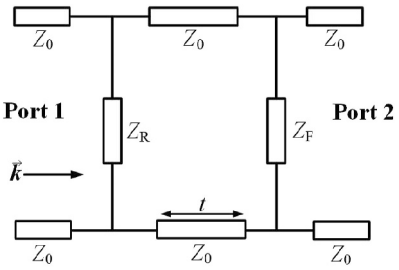

FIGURE 1 The equivalent circuit model (ECM) of the multilayer frequency selective rasorber (FSR).

Z_R is greater than $4.5Z_0$ and the imaginary part $|X|$ of Z_R is greater than $2.5Z_0$, it can be made $|S_{21}| > -0.5$ dB [18]. The imaginary part $|X|$ varies with frequency and is influenced by the equivalent inductance and capacitance. The infinity can be reached at the parallel resonant frequency, and a finitely considerable value can be achieved over a broad frequency range near the resonant frequency through the design of equivalent inductors and capacitors. Particularly, for a parallel LC (PLC) circuit composed of a solitary inductor L and a solitary capacitor C, the equivalent impedance is $Z_{\mathrm{PLC}} = j\omega L/(1 - \omega^2 LC)$, which is positively correlated with the inductance value L and negatively correlated with the capacitance value C. Hence, a wide transmission band can be obtained by using a parallel resonator comprising a large inductance and a small capacitance.

2.2 | The resistive layer design and miniaturisation

The resistive layer in Figure 2a is composed of meander cross-rings with lumped resistances, printed on a 0.3-mm thickness FR4 dielectric substrate with $\varepsilon_r = 4.4$ and $\tan\delta = 0.01$. The structure is bent to obtain a PLC circuit with an increased quality factor and inductance value. The parameters are as follows (unit: mm): $p = 9$, $l_1 = 8.2$, $l_2 = 8$, $w_1 = 6.1$, $w_2 = 5.9$, $m = 0.6$, and $n = 1.8$, and the lumped resistance value is 402 Ω. Figure 2b illustrates the ECM of the resistive layer. The physical structure of the resistive layer was established in Computer Simulation Technology (CST) software, followed by the size optimisation to achieve the desired absorption and transmission performance. Then, the ECM was built in Advanced Design System (ADS) software for S-parameter fitting in the desired bands. Ultimately, the correspondence is obtained between the L *and* C parameter values and the physical structure.

C_1 denotes the coupling capacitance between the meander cross-rings of neighbouring units along the electric field direction. L_1 denotes the inductance of the outer arms of the cross-ring. R is a lumped resistor soldered on the resistive layer, which is frequency-independent to obtain impedance matching. The combination of series RL_1C_1 generates the broad absorption band that is positioned below the transmission

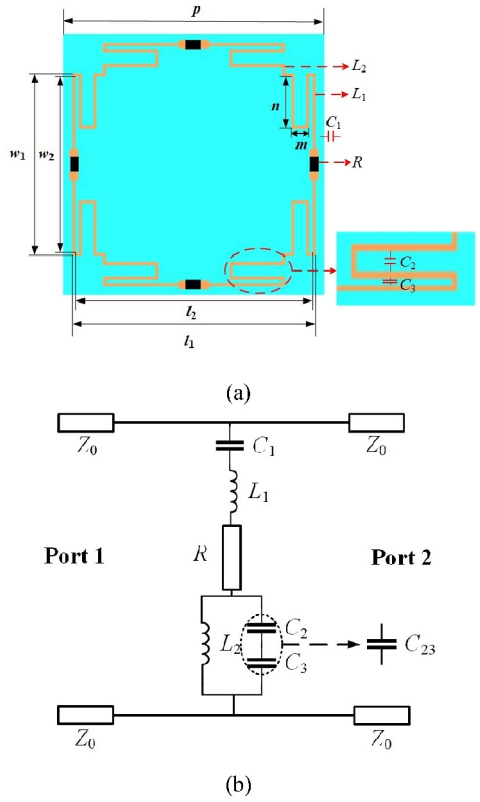

FIGURE 2 (a) Element of the resistive layer. (b) The equivalent circuit model (ECM) of the resistive layer.

band. L_2 denotes the inductance of the meander inner arms of the cross-ring. The inner arms are bent to extend the current path, thereby obtaining a large inductance value. C_2 represents the capacitance between the inner arms. C_3 represents the capacitance between the inner and outer arms. C_2 and C_3 are connected in series, and their equivalent capacitances are reduced by $C_{23} = C_2C_3/(C_2 + C_3)$. The larger inductance L_2 and the smaller capacitance C_{23} are connected in parallel to realise a wide transmission band. Using ADS simulation software for S-parameter fitting, the values of these circuit elements are acquired as follows: $C_1 = 0.124$ pF, $L_1 = 0.1$ nH, $R = 231\ \Omega$, $L_2 = 2.85$ nH, and $C_{23} = 0.038$ pF. The results obtained from CST simulation and ECM calculation for the transmission coefficients are compared in Figure 3, revealing that they are highly consistent. In the resistive layer, the transmission band with $|S_{21}| > -0.5$ dB spans from 13.23 to 18.38 GHz. In Figure 4a, b, it is evident that the frequency response of the resistive layer remains stable for transverse electric (TE) and transverse magnetic (TM) polarisations within the 0–30° range.

In addition, at the parallel resonant part of the resistive layer, the impedance is $Z_{PLC} = j\omega L_2/(1 - \omega^2 L_2 C_{23})$, which is infinite at the resonant frequency $f_0 = 1/2\pi\sqrt{L_2C_{23}}$. When the frequencies are lower than f_0, the value of the parallel L_2C_{23} is positive, which represents an inductive reactance. Since the value of C_{23} is very small, it can be ignored at low frequencies. In this case, the parallel resonant part acts as the load inductance, which causes the serial resonance of the

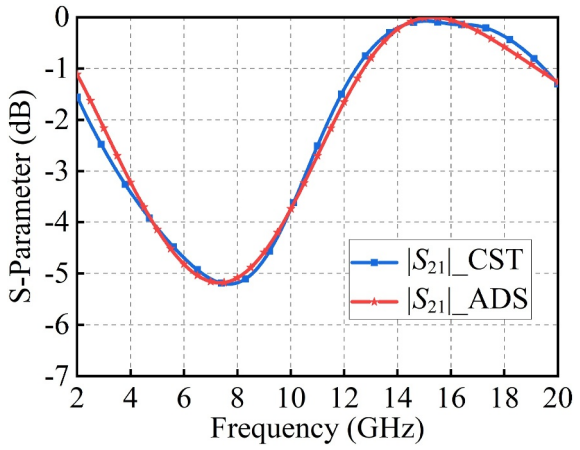

FIGURE 3 Transmission coefficients of the resistive layer obtained from the equivalent circuit model (ECM) calculation and CST simulation under normal incidence.

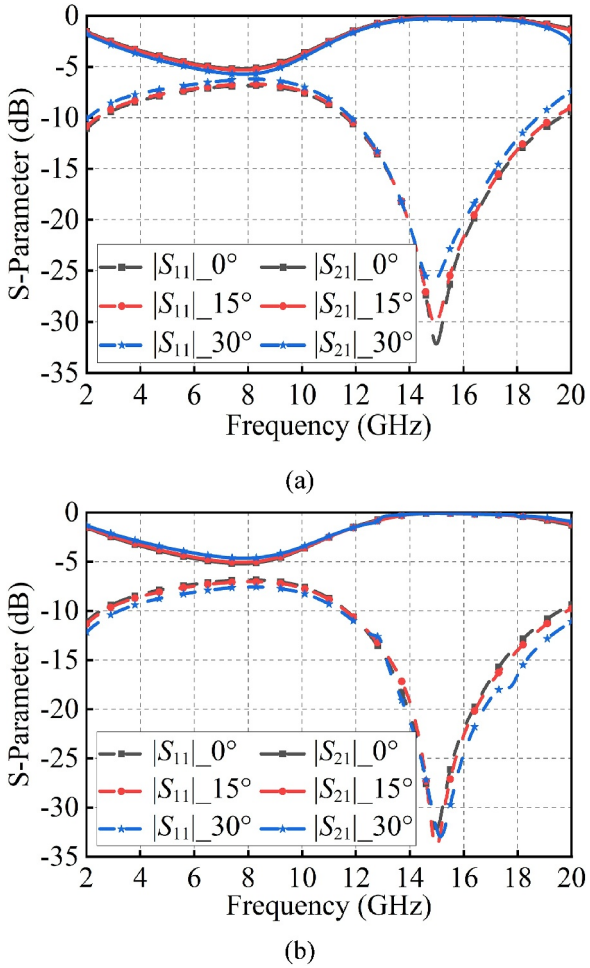

FIGURE 4 Simulated S-parameters of the resistive layer under oblique incidences. (a) TE polarisation. (b) TM polarisation.

resistive layer to be moved to the lower frequency. Hence, the unit dimension of the resistive layer is incredibly miniaturised to 0.11λ at the lowest operating frequency (3.66 GHz),

effectively avoiding the occurrence of grating lobes and improving angular stability.

2.3 | The bandpass frequency selective surface structural design

For obtaining the transmission band that matches the resistive layer, a triple-layer bandpass FSS is proposed. In the FSS, as illustrated in Figure 5a, the unit structure comprises two identical square rings that are coupled through a central metal grid, resulting in the formation of a second-order bandpass filter. The upper and lower square ring structures are equal, and the equivalent circuits of both layers consist of an inductor $L_{F1} = 0.1$nH and a capacitor $C_{F1} = 0.06$pF in series, which are obtained by parameters fitting in ADS. The middle metallic grid is equivalent to an inductor $L_{F2} = 0.6$nH. The two dielectric substrates with the thickness of h are equivalent to two transmission lines with a characteristic impedance of Z_{sub}. Two identical 0.8 mm TLA-6 dielectric substrates, both with $\varepsilon_r = 2.65$ and $\tan\delta = 0.001$, are utilised for printing the three metallic layers. The bandpass FSS is designed with the following construction parameters (unit: mm): $a = 3$, $b = 2.68$, $c = 1$, $d = 2.5$, and $h = 0.8$. The S-parameters of the bandpass FSS, derived from ECM and CST simulations under normal incidence, are illustrated in Figure 5b. It reveals that the passband of the FSS with $|S_{21}| > -0.5$ dB is from 12.31 to 18.18 GHz, which mainly covers the transmission band of the resistive layer.

3 | SIMULATION AND MEASUREMENT

The FSR depicted in Figure 6a is formed by the cascade of the above resistive layer and the bandpass FSS layer. One resistive layer unit corresponds to 3 × 3 FSS units because the dimension ratio of the resistive layer to the FSS layer is 3:1. There is an air layer with the thickness of $H = 7$ mm between them. In the ECM depicted in Figure 6b, Z_R is the characteristic impedance of the resistive layer and Z_F is the characteristic impedance of the bandpass FSS.

To better understand the physical working mechanism of the FSR, the surface current distributions are simulated at the centre frequencies of the absorption band $(f_1 = 6.7\text{GHz})$ and transmission band $(f_2 = 15.1\text{GHz})$ under TE polarisation. When the FSR is illuminated by a normally incident wave, a large amount of surface current is excited on the upper resistive layer at the absorption band in Figure 7a. The current flows along the outer arms of the cross-ring, indicating that series resonance has occurred. At this moment, the current passes through the lumped resistors loaded on the cross-ring, causing energy absorption. The surface current on the bandpass FSS layer is extremely weak, and no resonance occurs. This layer reflects the EM to the upper resistive layer, where it is absorbed. At the transmission band in Figure 7b, most of the surface current on the upper resistive layer flows along the folded inner arms of the cross-ring, indicating that parallel resonance has generated infinite impedance. Only a small amount of current passes through the resistors, resulting in minimal loss. Surface currents

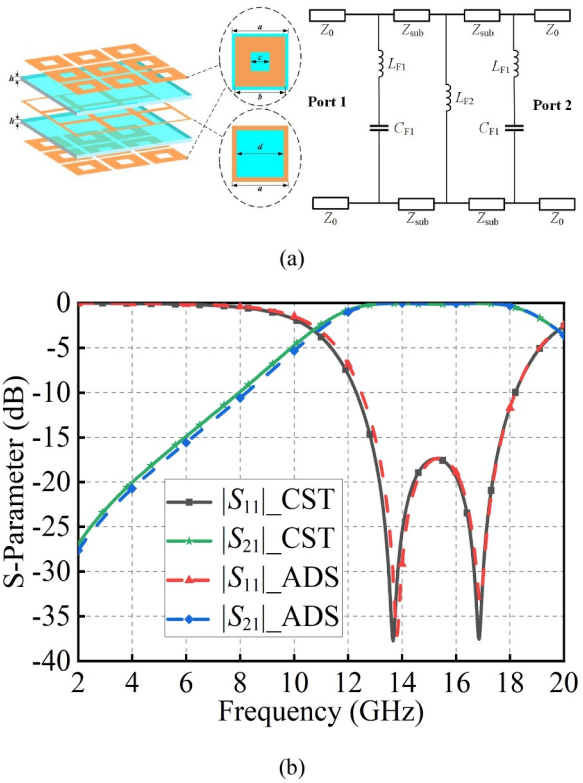

FIGURE 5 (a) Element of the bandpass frequency selective surface (FSS). (b) S-Parameter results of the FSS under normal incidence.

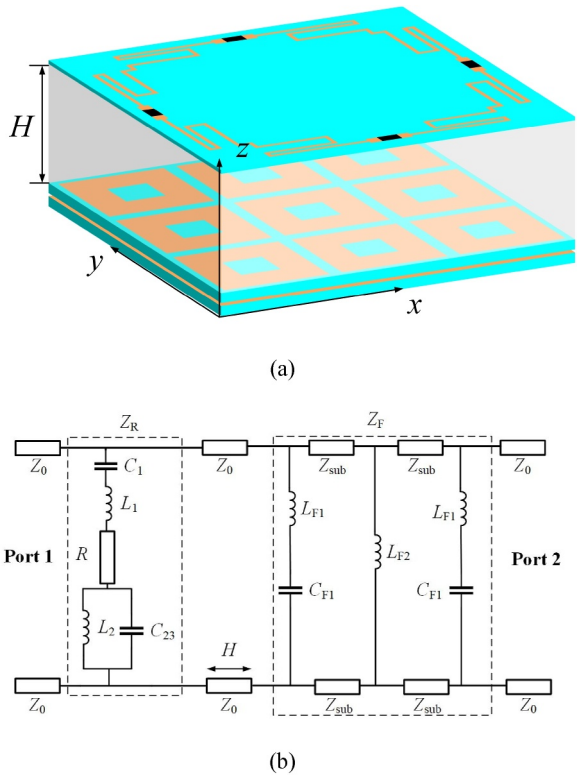

FIGURE 6 (a) Geometry of a unit cell of the frequency selective rasorber (FSR). (b) Equivalent circuit model (ECM) of the proposed FSR.

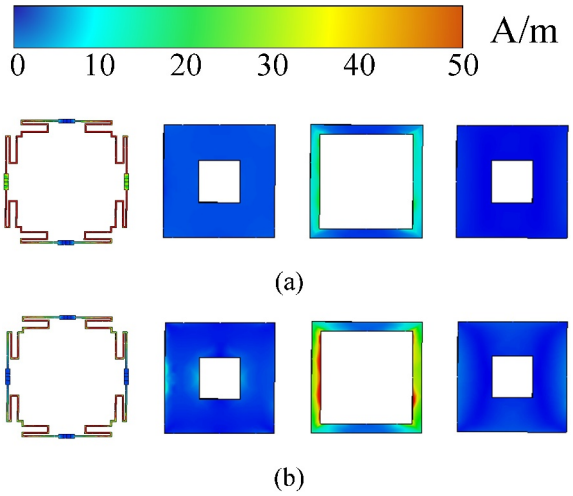

FIGURE 7 Surface current distribution diagram of frequency selective rasorber (FSR) under TE polarisation. (a) Absorptive frequency band. (b) Transmissive frequency band.

flow through all three layers of the FSS, showing that the upper and lower layers are coupled through the middle layer, producing parallel resonance and achieving in-band transmission.

The CST and ADS are utilised for simulating the S-parameters of the FSR when subjected to normal incidence in TE and TM polarisations, as depicted in Figure 8. The results obtained from CST simulation are in excellent concurrence with the ones obtained from ECM calculation performed using ADS. Because the structure of FSR is centrosymmetric, it has polarisation-insensitive characteristics. The transmission band with $|S_{21}| > -1$ dB spans from 12.22 to 17.93 GHz, demonstrating a 37.9% relative bandwidth. The minimum IL within this range is 0.16 dB. The absorption band with absorptance exceeding 90% is from 3.66 to 9.8 GHz, representing a 91.2% relative bandwidth.

Figure 9 displays the absorptive and transmissive characteristics of the FSR under the oblique incidence. In TE polarisation, the effect of absorption in the lower-frequency range gradually diminishes as the incident angle increases. However, even at an incident angle of 30°, the absorptance remains above 80%. In TM polarisation, the absorption bandwidth experiences a slight reduction as the incident angle increases. Nevertheless, the frequency response maintains a relatively stable profile within the scope of 0°–30° incident angles. Due to the miniaturisation of the FSR, it is evident that the transmission bands in TE and TM polarisations exhibit excellent angle stability with slight alteration in the bandwidth.

The validation of the simulation results was conducted through the fabrication and measurement of the FSR prototype, as depicted in Figure 10. The prototype size is 279 mm × 279 mm, including 31 × 31 resistive layer units and 93 × 93 bandpass FSS units. Using surface mount technology, 3844 chip resistors having a resistance of 402, a package of 0402, and an accuracy of 1% were mounted on the resistive layer. Using Printed Circuit Board technology, the FR4 dielectric substrate of 0.3 mm thickness ($\varepsilon_r = 4.4$) was utilised for printing the resistive layer, whereas the TLA-6 dielectric substrate of 0.8 mm thickness

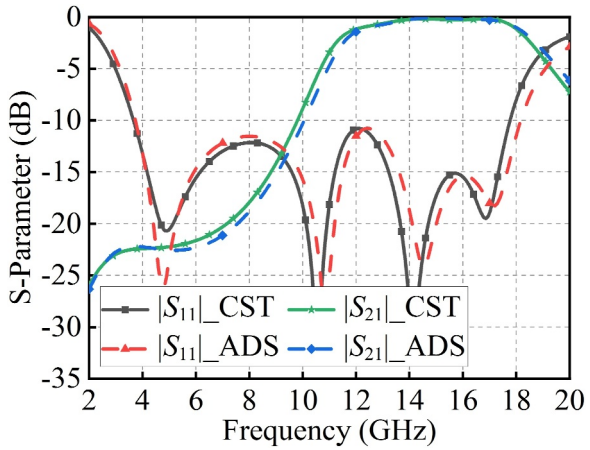

FIGURE 8 S-Parameters obtained from the CST simulation and equivalent circuit model (ECM) calculation under normal incidence.

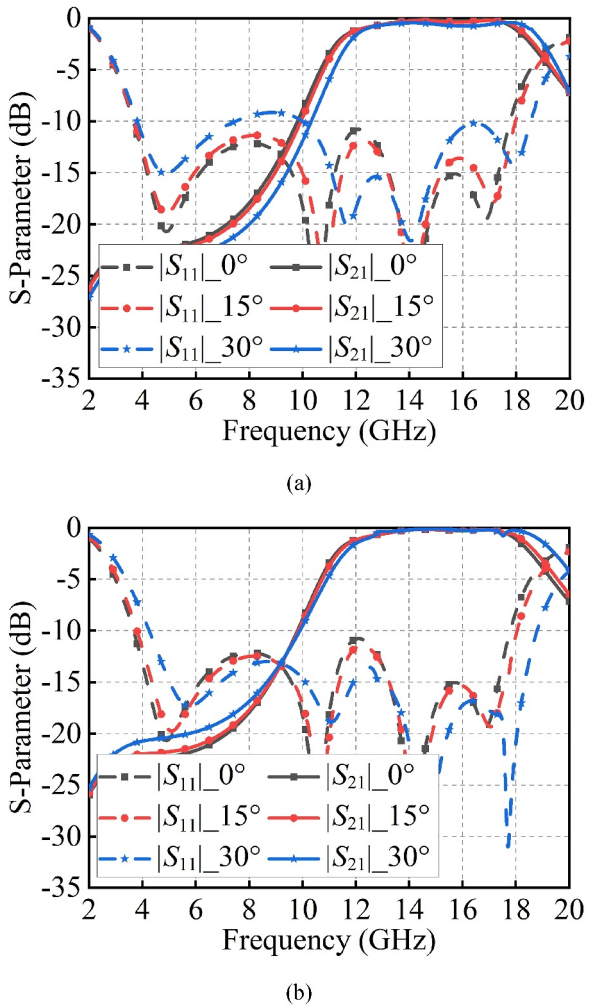

FIGURE 9 Simulated S-Parameter results of the frequency selective rasorber (FSR) under oblique incidences: (a) TE polarisation. (b) TM polarisation.

($\varepsilon_r = 2.65$) was utilised for printing the bandpass FSS layer. A layer of 7 mm thickness polymethacryimide (PMI) foam was placed between the two layers.

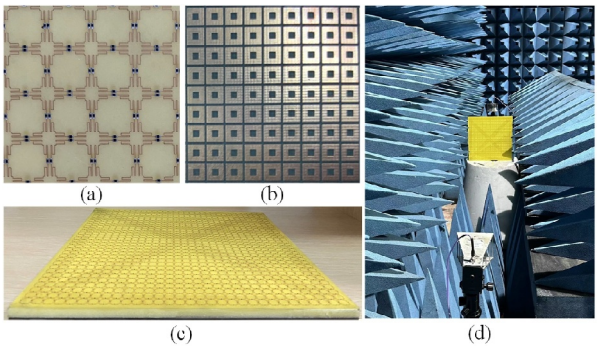

FIGURE 10 The fabrication and measurement of the frequency selective rasorber (FSR) prototype. (a) The resistive layer. (b) The bandpass frequency selective surface (FSS). (c) The integrated FSR. (d) Measurement of the FSR.

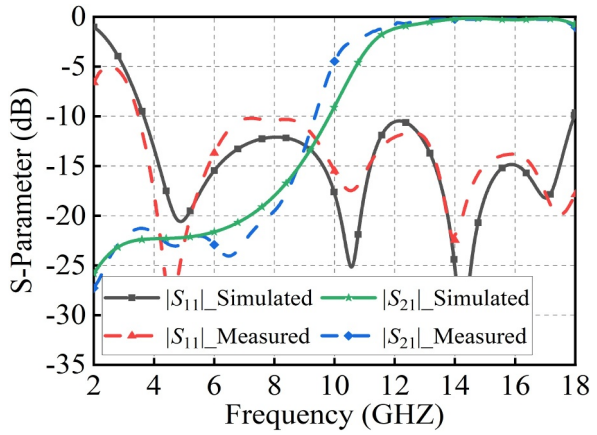

FIGURE 11 Simulated and measured S-Parameters of the frequency selective rasorber (FSR) under normal incidence.

The performance of the fabricated FSR was tested in a microwave anechoic chamber. The prototype was placed between two horn antennas (operating frequency range 2–18 GHz), which served as the transmitting and receiving antennas. The two horn antennas were connected to the two ports of the vector network analyser, and both were aligned with the centre of the sample. The transmission coefficients were measured with and without the FSR in place, and the difference between the processed results represented the characteristic curve of transmission bands.

When testing the reflection coefficient of the sample under normal incidence, only one horn antenna was needed to serve as both the transmitting and receiving antenna. The reflection coefficients of a metal plate with the same size as the FSR and of the prototype itself were measured separately. Using the time-domain gating function of the vector network analyser, the frequency-domain signal was converted into a time-domain signal to eliminate the effect of multiple reflections on the surface of the prototype or metal plate, yielding accurate measurements. The difference between the reflection coefficients of the metal plate and the prototype represented the reflection characteristic curve of the FSR.

The comparison between the S-parameters of simulation and measurement is presented in Figure 11. The measurement results indicate that the transmission band range of the $|S_{21}|$ greater than −1 dB is from 11.92 to 17.98 GHz. The absorption band with absorptance exceeding 90% is from 3.5 to 9.4 GHz. The variations primarily arise from the fabrication errors and the variability in the relative dielectric constant of the substrates. The air layer was replaced by the 7-mm thick PMI foam in order to prevent the weight of the dielectrics from depressing the surface of the resistance layer. The dielectric property of the used PMI is about 1.07–1.08, which is close to the air. Moreover, Figure 12 indicates the contrast between simulated and measured results for oblique incidence (30°), which are in good coincidence.

To better illustrate the advantages of the design, the performances of the proposed FSR are compared with other published FSRs, as shown in Table 1. The proposed FSR has

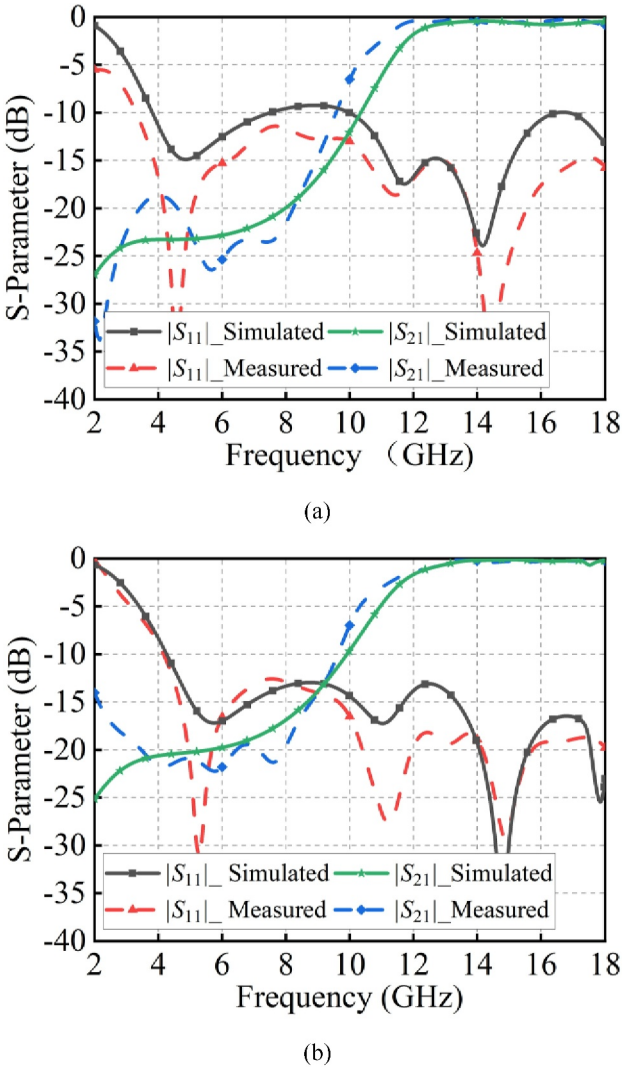

FIGURE 12 Simulated and measured S-Parameters of the frequency selective rasorber (FSR) prototype under oblique incidence. (a) TE-polarised 30° incidence. (b) TE-polarised 30° incidence.

TABLE 1 Performance comparison of the frequency selective rasorber (FSR) with a wide transmission band.

Ref.	Transmission band	Absorption band	Number of resistors	Thickness (mm)	Cell size (mm)	Angular stability (90% absorptivity)
[18]	8.3–11.07 GHz (28.6%)	2.4–7.1 GHz (98.9%)	6	15.35	12	30°
[19]	9.38–12.48 GHz (28.4%)	3.88–7.63 GHz (65.2%)	4	10.508	14	45°
[20]	14.3–17.4 GHz (19.6%)	3.2–10.7 GHz (107.9%)	4	11	8	30°
[21]	5–7 GHz (33.3%)	1.6–4.3 GHz (91.5%)	8	18.59	30	30°
This work	12.22–17.93 GHz (37.9%)	3.66–9.8 GHz (91.2%)	4	8.9	9	30°

the widest relative bandwidth in the transmission band under the condition of relatively good absorptions. Furthermore, the FSR has the simple structure according to the less lumped resistors used in each unit and more compact cell size.

4 | CONCLUSION

The paper illustrates the design of a miniaturised FSR that exhibits a wide transmission band. By cascading the resistive layer and FSS, the FSR achieves a transmission band with IL than −1 dB and an absorption band with absorptance exceeding 90%. Great angular stability under oblique incidence is also demonstrated and the prototype is measured to validate the design. The proposed FSR is applicable for radar radomes, effectively improving the all-around stealth capability and survivability of radar systems in the battlefield.

AUTHOR CONTRIBUTIONS

Ruofeng Xu: Conceptualisation; data curation; investigation; methodology; resources; writing—review & editing. **Jing Wang**: Conceptualisation; data curation; formal analysis; writing—original draft. **Xianglin Kong**: Methodology; validation. **Bingmei Zhang**: Resources; investigation. **Jun Wang**: Validation. **Shengjun Zhang**: Methodology. **Xiaochun Liu**: Project administration; writing—review & editing. **Lei Zhao**: Supervision; visualisation.

ACKNOWLEDGEMENTS

This work was supported by the National Natural Science Foundation of China under Grant 51507176, 61771226, 62201575.

CONFLICT OF INTEREST STATEMENT

The authors declare no conflicts of interest statement.

DATA AVAILABILITY STATEMENT

The data that support the findings of this study are available from the corresponding author upon reasonable request.

ORCID

Ruofeng Xu https://orcid.org/0000-0003-2627-3624
Jun Wang https://orcid.org/0000-0001-6459-5830
Lei Zhao https://orcid.org/0000-0003-0975-0943

REFERENCES

1. Costa, F., Monorchio, A.: A frequency selective radome with wideband absorbing properties. IEEE Trans. Antennas Propag. 60(6), 2740–2747 (2012). https://doi.org/10.1109/tap.2012.2194640
2. Yu, W.L., et al.: Dual-polarized band-absorptive frequency selective rasorber using meander-line and lumped resistors. IEEE Trans. Antennas Propag. 67(2), 1318–1322 (2019). https://doi.org/10.1109/tap.2018.2883643
3. Yu, W.L., et al.: Miniaturised band-absorptive frequency selective rasorbers with wide absorption band. IET Microw., Antennas Propag. 13(11), 1777–1781 (2019). https://doi.org/10.1049/iet-map.2018.6170
4. Zhou, H., et al.: Experimental demonstration of an absorptive/transmissive FSS with magnetic material. IEEE Antennas Wireless Propag Lett. 13, 114–117 (2014). https://doi.org/10.1109/lawp.2013.2296992
5. Chen, Q., et al.: Design of absorptive/transmissive frequency-selective surface based on parallel resonance. IEEE Trans. Antennas Propag. 2017 Sept 65(9), 4897–4902 (2017). https://doi.org/10.1109/tap.2017.2722875
6. Chen, Q., et al.: Design of absorptive frequency selective surface with good transmission at high frequency. Electron. Lett. 51(12), 885–886 (2015). https://doi.org/10.1049/el.2015.0228
7. Xiu, X., et al.: Low-profile dual-polarization frequency-selective rasorbers based on simple-structure lossy cross-frame elements. IEEE Antennas Wireless Propag Lett. 17(6), 1002–1005 (2018). https://doi.org/10.1109/lawp.2018.2829022
8. Xing, Q.J., et al.: A wideband frequency-selective rasorber with rectangular spiral resonators. IEEE Antennas Wireless Propag Lett. 21(8), 1688–1692 (2022). https://doi.org/10.1109/lawp.2022.3177740
9. Ye, H., et al.: High-selectivity frequency-selective rasorber based on low-profile bandpass filter. IEEE Antennas Wireless Propag Lett. 20(2), 150–154 (2021). https://doi.org/10.1109/lawp.2020.3041761
10. Zargar, M.M., et al.: Frequency-selective rasorber based on high-Q minkowski fractal-shaped resonator for realizing a low radar cross-section radiating system. IEEE Trans. Electromagn. Compat 64(5), 1574–1584 (2022). https://doi.org/10.1109/temc.2022.3179514
11. Jia, Y.X., et al.: Design of a hybrid frequency selective rasorber with wideband reflection suppression. IEEE Antennas Wireless Propag Lett. 22(2), 293–297 (2023). https://doi.org/10.1109/lawp.2022.3209549
12. Xue, K., Zhai, H.Q.: A compact ultrawideband frequency selective rasorber with hybrid 2-D and 3-D structure. IEEE Antennas Wireless Propag Lett. 2022 Sept 21(9), 1872–1876 (2022). https://doi.org/10.1109/lawp.2022.3183615
13. He, W., et al.: A compact ultrawideband circularly polarized antenna array with shared partial patches. IEEE Antennas Wireless Propag Lett. 20(12), 2280–2284 (2021). https://doi.org/10.1109/lawp.2021.3107218
14. Shi, Y.P., et al.: An ultrawideband compact magneto-electric dipole antenna and its coupled array. IEEE Antennas Wireless Propag Lett. 22(7), 1662–1666 (2023). https://doi.org/10.1109/lawp.2023.3258414
15. Chen, X., Li, K.: Ultrathin and flexible ultrawideband antenna array based on integrated impedance matching line. IEEE Antennas Wireless Propag Lett. 22(5), 960–964 (2023). https://doi.org/10.1109/lawp.2022.3229108

16. Li, D., et al.: A low-profile broadband bandpass frequency selective surface with two rapid band edges for 5G near-field applications. IEEE Trans. Electromagn. Compat 59(2), 670–676 (2017). https://doi.org/10.1109/temc.2016.2634279
17. Al-Journayly, M., Behdad, N.: A new technique for design of low-profile, second-order, bandpass frequency selective surface. IEEE Trans. Antennas Propag. 57(2), 452–459 (2009)
18. Chen, Q., et al.: Miniaturized frequency-selective rasorber with a wide transmission band using circular spiral resonator. IEEE Trans. Antennas Propag. 67(2), 1045–1052 (2019). https://doi.org/10.1109/tap.2018.2880043
19. Guo, M., et al.: Wide transmission band frequency-selective rasorber based on convoluted resonator. IEEE Antennas Wireless Propag Lett. 19(5), 846–850 (2020). https://doi.org/10.1109/lawp.2020.2981836
20. Sheng, X.J., Gao, X., Liu, N.: Design of frequency selective rasorber with wide transmission/absorption bands. J. Phys. D Appl. Phys. 53(9), 09LT01 (2020). https://doi.org/10.1088/1361-6463/ab5a22
21. Wang, Z.F., et al.: Wideband transmissive frequency-selective absorber. IEEE Antennas Wireless Propag Lett. 18(7), 1443–1447 (2019). https://doi.org/10.1109/lawp.2019.2919633

How to cite this article: Xu, R., et al.: A miniaturised frequency selective rasorber with wide transmission band. IET Microw. Antennas Propag. 1–8 (2024). https://doi.org/10.1049/mia2.12543